

Sampling in the multicanonical ensemble: Small He clusters in W

Thomas Vogel* and Danny Perez

Theoretical Division (T-1), Los Alamos National Laboratory, Los Alamos, NM 87545, USA

(Dated: April 3, 2014)

We carry out generalized-ensemble molecular dynamics simulations of the formation of small Helium (He) clusters in bulk Tungsten (W), a process of practical relevance for fusion energy production. We calculate formation free energies of small Helium clusters at temperatures up to the melting point of W, encompassing the whole range of interest for fusion-energy production. From this, parameters like cluster break-up or formation rates can be calculated, which help to refine models of microstructure evolution in He-irradiated Tungsten.

I. INTRODUCTION

Many challenges have to be addressed to enable energy production from nuclear fusion. While issues related to plasma stability are considerable, it is increasingly clear that material stability in the extreme conditions typical of the operation of such reactor are critical. For example, tungsten is a leading candidate for the construction of plasma-facing components [1, 2], due to comparatively favorable properties such as very high melting point, low sputtering yield, etc. One serious problem however is that the irradiation of W by Helium ions incoming from the plasma can cause serious modifications in the microstructure of the exposed materials [3–7]. In particular, He bubbles nucleating from small He clusters inside the material can grow, coalesce, and burst, severely damaging the surface. Since small helium clusters (of sizes $N \simeq 7$) serve as nuclei of such bubbles, it is of great technological interest to investigate the behavior of such clusters in W [8, 9].

In this paper we focus on one key detail of such a study, the determination of the formation free energy of He clusters. We perform molecular dynamics (MD) simulations in the multicanonical ensemble [10, 11] and measure the distributions of He cluster compositions. We obtain the simulation weights through STMD (Statistical Temperature MD) [12], a molecular dynamics protocol derived from the Wang–Landau approach [13].

II. SIMULATION PROTOCOL

A. Theory review and estimation of simulation weights

The multicanonical (muca) ensemble [14] is the ensemble where the distribution of potential energies (or any other reaction coordinate/order parameter) becomes flat. In practice, the simulation weights $w_{muca}(E)$ (which would be the Boltzmann factors for the canonical ensemble) required to sample from this ensemble, be it using Monte Carlo (MC) or molecular dynamics (MD) methods, are not known *a priori* and have to be determined first. Since $w_{muca}(E)$ is related to the density of states $g(E)$ via the ensemble-defining condition

$$P_{muca}(E) \propto g(E) w_{muca}(E) \stackrel{!}{=} \text{const.}, \quad (1)$$

one can obtain thermodynamic averages at *any* temperatures by reweighting measured data with respect to the simulation weights, as will be shown below.

For a muca MD simulation one can, in principle, use any canonical integrator at a reference temperature T_0 using an effective potential V_{muca} leading to the flat, multicanonical distribution instead of the usual, raw potential (which would lead to a canonical distribution). Introducing the entropy $S(E) = k_B \ln g(E)$ (where k_B is the Boltzmann constant), one defines from Eq. (1) the effective potential $V_{muca}(E)$:

$$w_{muca}(E) \propto e^{-k_B^{-1} S(E)} =: e^{-V_{muca}(E)/(k_B T_0)}, \quad \text{and} \quad V_{muca}(E) = T_0 S(E). \quad (2)$$

Interatomic forces are then calculated via the gradient of the effective potential with respect to the particle coordinates:

$$f_i^{muca} = -\frac{dV_{muca}(S(E(q_1, \dots, q_{3n})))}{dq_i} = -T_0 \frac{\partial S(E)}{\partial E} \frac{dE(q_1, \dots, q_{3n})}{dq_i}. \quad (3)$$

* E-mail: tvogel@lanl.gov

Since the last term equals minus the canonical (conventional) forces f_i and the second one defines a temperature via the thermodynamic relation $T(E)^{-1} := \partial S(E)/\partial E$, we can write the multicanonical forces simply as rescaled canonical forces:

$$f_i^{muca} = \frac{T_0}{T(E)} f_i. \quad (4)$$

The function $T(E)$ is still unknown and estimating it is equivalent to estimating $g(E)$, $V_{muca}(E)$, or $S(E)$. Following the Wang–Landau (WL) scheme for MC simulations, Kim *et al.* proposed a method (STMD [12]) to estimate $T(E)$ during a MD simulation. Once the estimator $T'(E, t)$ has converged, $S(E)$ can be estimated by direct numerical integration. In STMD, one would start (at simulation time $t = 0$) with a constant initial guess $T'(E, t = 0) = T_{init}$ (which is equivalent to a canonical MD simulation at T_{init}) and update $T'(E, t + \Delta t)$ via

$$T'(E_{act\pm 1}, t + \Delta t) = \frac{T'(E_{act\pm 1}, t)}{1 \mp \delta_\beta T'(E_{act\pm 1}, t)}, \quad (5)$$

with $\delta_\beta := k_B \ln f_{WL}/2\Delta E$. We assume that $T'(E, t)$ was binned (with ΔE being the energy bin width) and the underlying WL procedure is just the update of the single bin containing the current energy E_{act} via $\ln g'(E_{act}, t + \Delta t) = \ln g'(E_{act}, t) + \ln f_{WL}$. f_{WL} is usually called the modification factor and decreases during the simulation as in the WL scheme [13], $y'(x)$ always refers to an estimator for the true function $y(x)$. The derivation of Eq. (5) is straightforward and details can be found in the original publications [12]. It can be noted that this scheme leads to exactly the same dynamics as obtained in a metadynamics simulation if $T'(E, t)$ is updated on the basis of Gaussian kernel functions, provided all method parameters are chosen consistently [11].

B. Physical system, simulation details, and measurements

The systems we are simulating consists of 432 Tungsten ($6 \times 6 \times 6$ W unit cells) and N Helium (He) atoms, which interact via embedded atom potentials (W–W interactions: [15], modified in [16]; He–He interactions: [17], modified in [18]; He–W interactions: [16]). For illustration, Fig. 1 shows ground-state configurations for $N = 2, 4, 6, 8,$ and 10 , also showing the effect of small He clusters on the structure of the surrounding W. Technically, we perform simulations for $2 \leq N \leq 8$ in the temperature range $T_{min} = 100 \text{ K} \leq T(E) \leq T_{max} = 3700 \text{ K}$. Outside this range, we effectively perform canonical simulations at T_{min} and T_{max} , respectively, by holding $T(E)$ fixed at those values (cp. [12]). However, it is almost impossible to obtain reliable data regarding free-energy differences for very low temperatures anyway since the probability of observing free He atoms vanishes (see below). Therefore, in practice, we require the histogram to be flat only for $T > 300 \text{ K}$ in order to save time. The reference temperature $T_0 = 2200 \text{ K}$ is imposed using a Langevin thermostat and the particle positions evolve following the stochastic Velocity-Verlet integration scheme [19]. The simulation box has a linear size of 18.991 \AA , i.e., we simulate at constant volume, and periodic boundary conditions are applied in all three directions.

After having estimated $T(E)$ via STMD, we fix it and perform muca MD simulations based on Eq. (4). During these production runs, we measure the 2-dimensional histograms $H(E, Q)$, where Q is the He-cluster composition. In practice, the values of Q are just integers uniquely identifying every possible arrangement of the N He atoms into clusters (including the trivial cluster of size 1). For $N = 2$, there exist $c(N) = 2$ such compositions: two single He atoms (o-o) or one cluster of two (oo). For $N = 3$, there are $c(N) = 3$ compositions (o-o-o; oo-o; ooo), $c(4) = 5$ (o-o-o-o; o-o-oo; o-ooo; oo-oo; oooo), $c(5) = 7$, $c(6) = 11$, and so on. For large N , the number of compositions $c(\sqrt{N})$ grows exponentially [20]. An off-lattice version of the Hoshen–Kopelman algorithm [21] was implemented to uniquely

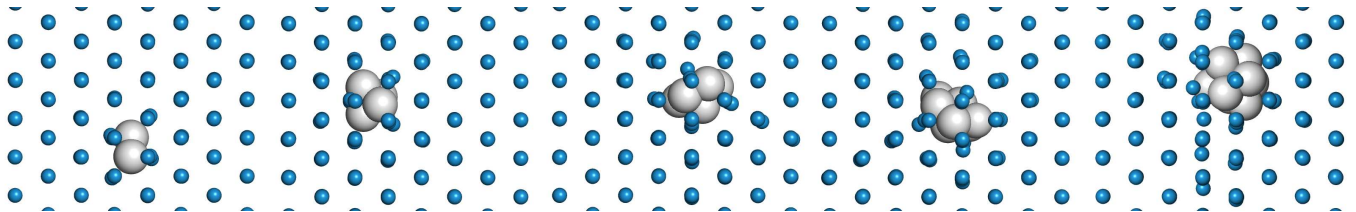


FIG. 1. Ground-state structures for $N = 2, 4, 6, 8,$ and 10 (from left to right) He atoms in bulk W. While the cluster of two atoms (left) only slightly and locally affects the W structure, larger clusters also disturb next-neighbor positions and eventually eject W interstitial crowdions, leading to the nucleation of a nano-bubble (right).

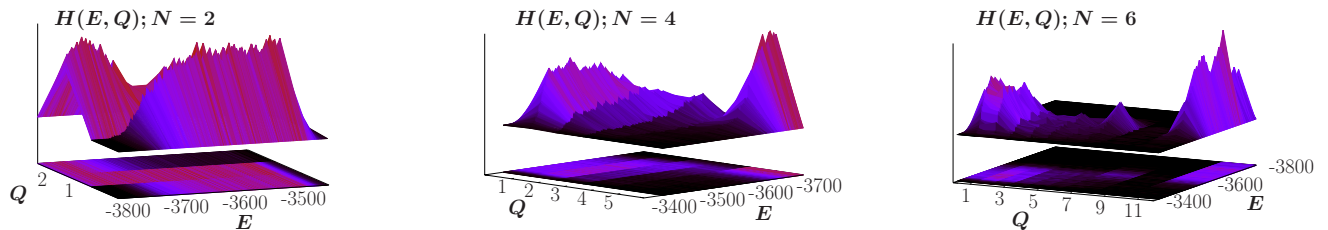


FIG. 2. Examples of two-dimensional histograms of energy (E) and cluster composition (Q) as measured during multicanonical production runs.

identify the cluster distribution and measure Q . Figure 2 shows three examples of histograms $H(E, Q)$ measured in the production runs. We perform many independent runs for each value of N and use the combined histograms for further calculations. All simulations ran on single CPUs, a small cluster machine (less than 100 CPUs) was used to perform independent production runs in parallel. Estimation of $T(E)$ took about one week for each N , production ran for a few days.

III. RESULTS

Canonical distributions of the cluster compositions $P_T^{can}(Q)$ for all temperatures T are obtained by reweighting, i.e., by dividing by the applied simulation weights, multiplying with the Boltzmann weights, and summing over all energies:

$$P_T^{can}(E, Q) = w_{muca}^{-1} H(Q, E) e^{-E/k_B T}, \quad P_T^{can}(Q) = \sum_E P_T^{can}(E, Q), \quad (6)$$

where we use a sum instead of an integral because of the discrete nature of the energy bins. With these distributions in hand, it is straightforward to calculate the probabilities $p_Q(T)$ for certain cluster compositions to occur at a given temperature T . We plot $p_Q(T)$ for $N = 2, 3, 4$, and 6 in Fig. 3. The high-temperature boundary in the plots corresponds to the melting temperature of Tungsten. For $N = 2$, we see that for $T < 1000$ K isolated He atoms are basically never observed, while at $T \approx 2000$ K we find single atoms and cluster with about the same probability. Furthermore, it appears that He cluster become more stable as N increases. For example, single He atoms start to split off a cluster of size $N = 4$ at $T \approx 1500$ K. For $N = 6$, single He atoms are basically never found at any temperature $T \lesssim 2500$ K. Even for the highest temperatures, the only relevant compositions are (ooooo) and (o-oooo). However, note that these probabilities depend on the volume of the simulation cell and might be different for constant pressure simulations, for example.

The probabilities $p_Q(T)$ provide a means to calculate free energy differences. Following Kindt [20], we write the free energy of a He cluster of size s as $F_s(T) = -k_B T \ln q_s$, where q_s is the partition function of that cluster (in particular, q_1 is the partition function of a free He atom). The free energy difference for the complete breakup of a cluster of size s into s single atoms, for example, then reads:

$$F_s - sF_1 = -k_B T \ln (q_s/q_1^s). \quad (7)$$

Analogously, one defines free energy changes corresponding to the split-off of a single atom from a cluster of size s as:

$$F_s - F_{(s-1)} - F_1 = -k_B T \ln (q_s/q_{(s-1)}q_1). \quad (8)$$

The ensemble-averaged numbers ($\langle n_s \rangle$) of clusters of size s are functions of the partition functions q_s [20], hence we can write the free energy differences as functions of the $\langle n_s \rangle$ (calculations not shown). Since the $\langle n_s \rangle$ are related to the probabilities $p_Q(T)$, ratios of cluster partition functions are related to ratios of the probabilities to observe certain cluster compositions. For example:

$$\frac{q_2}{q_1^2} = \frac{P_{(oo)}}{2! p_{(o-o)}}, \quad \frac{q_3}{q_2 q_1} = \frac{P_{(ooo)}}{p_{(o-oo)}}, \quad \frac{q_3}{q_1^3} = \frac{P_{(ooo)}}{3! p_{(o-o-o)}}, \quad (9)$$

and so on. We show the formation free energies corresponding to Eqs. (7) and (8) for $N = 3$ and 4 in Fig. 4 as illustrations. For low temperatures, we obtain relatively large errors bars, the origin of which becomes clear when looking at Eqs. (9) and the data in Fig. 3. For $N = 4$ and $T = 1600$ K, for example, the composition (o-o-o) is

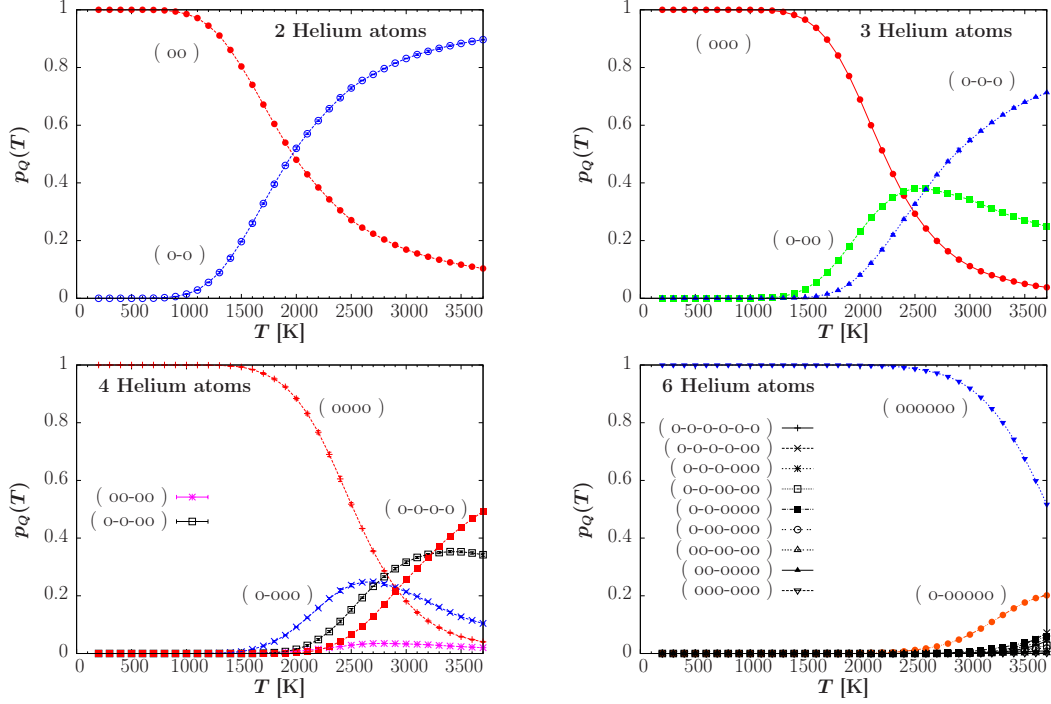


FIG. 3. Probabilities $p_Q(T)$ for cluster compositions to occur at different temperatures. Error bars are shown for all data, but might be smaller than the symbols.

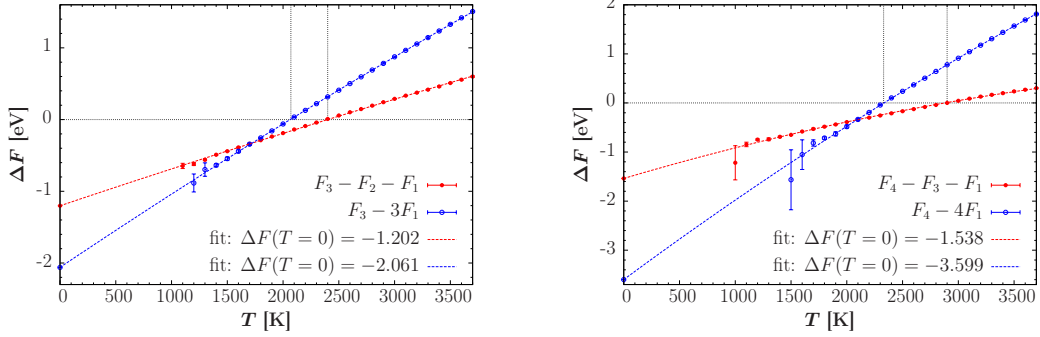


FIG. 4. Formation free energy differences for different temperatures calculated from data shown in Fig. 3. Left: 3 He atoms, right: 4 He atoms.

extremely rare, the ratio $p_{(oooo)}/p_{(o-o-o-o)}$ being larger than 10^6 . For even lower temperatures, it is not practical to calculate reliable free energy differences in this way. However, at $T = 0$, the free energy difference reduces to the difference of the potential energies of the ground state structures. This point can be used to obtain a fit to the free energy over the whole temperature range.

IV. OUTLOOK

Using differences in formation free energies one can calculate cluster break-up or formation rates, and estimate effective capture radii. The calculated cluster formation rates, for example, are shown in [8] and were validated by independent measurements from canonical molecular dynamics simulations at fixed temperatures. These quantities are essential to parameterize higher level models of microstructure evolution in low energy He irradiated Tungsten [9], and to understand and optimize the behavior of W in the extreme conditions of relevance to fusion energy production.

ACKNOWLEDGMENTS

Funding for this research was provided by Los Alamos National Laboratory's (LANL) Laboratory Directed Research and Development ER program. LANL is operated by Los Alamos National Security, LLC, for the National Nuclear Security Administration of the U.S. DOE under Contract DE-AC52-06NA25396. LA-UR-14-21924 assigned.

-
- [1] G. Janeschitz, J. Nucl. Mater. **290**, 1 (2001).
 - [2] H. Bolt, V. Barabash, W. Krauss, J. Linke, R. Neu, S. Suzuki, N. Yoshida, and ASDEX Upgrade Team, J. Nucl. Mater. **329**, 66 (2004).
 - [3] D. Nishijima, M.-Y. Ye, N. Ohno, and S. Takamura, J. Nucl. Mater. **329**, 1029 (2004).
 - [4] K. Tokunaga, M. J. Baldwin, R. P. Doerner, N. Noda, Y. Kubota, N. Yoshida, T. Sogabe, T. Kato, and B. Schedler, J. Nucl. Mater. **337**, 887 (2005).
 - [5] S. Takamura, N. Ohno, D. Nishijima, and S. Kajita, Plasma Fusion Res. **1**, 51 (2006).
 - [6] M. J. Baldwin and R. P. Doerner, Nucl. Fusion **48**, 035001 (2008).
 - [7] M. J. Baldwin, R. P. Doerner, D. Nishijima, K. Tokunaga, and Y. Ueda, J. Nucl. Mater. **390**, 886 (2009).
 - [8] D. Perez, T. Vogel, and B. P. Uberuaga, *Diffusion and transformation kinetics of small helium clusters in bulk tungsten*, submitted to Phys. Rev. B (2014).
 - [9] T. Faney, D. Xu, and B. D. Wirth, *Spatially-dependent cluster dynamics modeling of microstructure evolution in low energy helium irradiated tungsten*, submitted to Modelling Simul. Mater. Sci. Eng. (2014).
 - [10] U. H. E. Hansmann, Y. Okamoto, and F. Eisenmenger, Chem. Phys. Lett. **259**, 321 (1996).
 - [11] C. Junghans, D. Perez, and T. Vogel, *Molecular Dynamics in the Multicanonical Ensemble: Equivalence of Wang–Landau Sampling, Statistical Temperature Molecular Dynamics, and Metadynamics*, submitted to J. Chem. Theory Comput. (2014); arXiv:1401.6184.
 - [12] J. Kim, J. E. Straub, and T. Keyes, Phys. Rev. Lett. **97**, 050601 (2006); J. Chem. Phys. **126**, 135101 (2007).
 - [13] F. Wang and D. P. Landau, Phys. Rev. Lett. **86**, 2050 (2001); Phys. Rev. E **64**, 056101 (2001).
 - [14] B. A. Berg and T. Neuhaus, Phys. Lett. B **267**, 249 (1991); Phys. Rev. Lett. **68**, 9 (1992).
 - [15] G. J. Ackland and R. Thetford, Phil. Mag. A **56**, 15 (1987).
 - [16] N. Juslin and B. D. Wirth, J. Nucl. Mater. **432**, 61 (2013).
 - [17] D. E. Beck, Mol. Phys. **14**, 311 (1968); Mol. Phys. **15**, 332 (1968).
 - [18] K. Morishita, R. Sugano, B. D. Wirth, and T. Diaz de la Rubia, Nucl. Instrum. Methods Phys. Res. B **202**, 76 (2003).
 - [19] S. Melchionna, J. Chem. Phys. **127**, 044108 (2007).
 - [20] J. T. Kindt, J. Chem. Theory Comput. **9**, 147 (2013).
 - [21] J. Hoshen and R. Kopelman, Phys. Rev. B **14**, 3438 (1976).